Bias and temperature dependence of the 0.7 conductance anomaly in quantum point contacts

A. Kristensen, H. Bruus, A. E. Hansen, J. B. Jensen, P. E. Lindelof, C. J. Marckmann, J. Nygård, and C. B. Sørensen
Niels Bohr Institute, Ørsted Laboratory, Universitetsparken 5, DK-2100 Copenhagen, Denmark

F. Beuscher, A. Forchel, and M. Michel
Technische Physik, Universität Würzburg, Am Hubland, D-97074 Würzburg, Germany
(Received 4 May 2000)

The 0.7 $(2e^2/h)$ conductance anomaly is studied in strongly confined, etched GaAs/GaAlAs quantum point contacts, by measuring the differential conductance as a function of source-drain and gate bias as well as a function of temperature. We investigate in detail how, for a given gate voltage, the differential conductance depends on the finite bias voltage and find a so-called self-gating effect, which we correct for. The 0.7 anomaly at zero bias is found to evolve smoothly into a conductance plateau at 0.85 $(2e^2/h)$ at finite bias. On varying the gate voltage the transition between the 1.0 and 0.85 $(2e^2/h)$ plateaus occurs for definite bias voltages, which define a gate-voltage-dependent energy difference Δ. This energy difference is compared with the activation temperature T_a extracted from the experimentally observed activated behavior of the 0.7 anomaly at low bias. We find $\Delta = k_B T_a$, which lends support to the idea that the conductance anomaly is due to transmission through two conduction channels, of which the one with its subband edge Δ below the chemical potential becomes thermally depopulated as the temperature is increased.

I. INTRODUCTION

The quantized conductance through a narrow quantum point contact (QPC), discovered in 1988,[1,2] is one of the key effects in mesoscopic physics. The quantization of the conductance in units of the spin degenerate conductance quantum $G_2 = 2e^2/h$ can be explained within a single-particle Fermi-liquid picture in terms of the Landauer-Büttiker formalism as, in the simplest case, adiabatic transport through the constriction. For a review, see Ref. 3.

Since 1995 several experiments[4–7] on quantum wires and point contacts have revealed deviations from this integer quantization $G = nG_2$, $n = 1,2,3, \ldots$. In particular, the 0.7 conductance anomaly, noted[8] for the first time in 1991 but first studied in detail in 1996,[7] poses one of the most intriguing and challenging puzzles in the field, both experimentally and theoretically.[9–18] This anomaly is a narrow plateau, or in some cases just a shoulderlike feature, clearly visible at the low density side of the first conductance plateau in the dependence of the conductance G on a gate voltage that tunes the width and electron density of the QPC. For low bias voltage the conductance value of the anomalous plateau is around $0.7G_2$, giving rise to the name of the phenomenon. The 0.7 anomaly has been recorded in many QPC transport experiments involving different materials, geometries, and measurement techniques.[7,13,19]

In this paper, we present experimental evidence that the 0.7 conductance anomaly is associated with a density-dependent energy difference separating two transmission channels. We reach this conclusion by measuring both the temperature and the source-drain bias voltage dependence of the differential conductance $G = dI/dV_{\mathrm{sd}}$, through shallow-etched QPC's.

The outline of the paper is as follows. In Sec. II we describe the fabrication of the six samples to be investigated. In the following all detailed results on the conductance of the QPC's are shown solely for sample A, and only toward the end of the paper are the main results from all samples shown. In Sec. III we discuss the lateral confinement potential defining the QPC, and we focus in particular on the fact that this potential is controlled by two independent variables: the gate bias and the source-drain bias. Then follows in Sec. IV the results from finite source-drain bias spectroscopy, and the important energy difference Δ is introduced. We deal with the temperature dependence of the zero-bias conductance in Sec. V and introduce the activation energy T_A. The main result is obtained in Sec. VI where we show that $\Delta = k_B T_A$ for all six samples. A short conclusion is given in Sec. VII.

II. THE SHALLOW-ETCHED SAMPLES

The quantum point contacts were all fabricated on modulation doped GaAs/GaAlAs heterostructures grown by molecular beam epitaxy (MBE). The layer sequence is 1 μm GaAs buffer, 20 nm $Ga_{0.7}Al_{0.3}As$ spacer, 40 nm $Ga_{0.7}Al_{0.3}As$ barrier layer with a Si concentration of 2×10^{24} m^{-3}, and 10 nm undoped GaAs cap layer. The carrier density is 2×10^{15} m^{-2} and the mobility is 100 m^2/V s, measured in the dark at a temperature of 4.2 K.

The samples were processed with a 20×100 μm^2 mesa, etched to 100 nm, and AuGeNi Ohmic contacts to the two-dimensional electron gas (2DEG) were formed by conventional UV lithography, lift-off, and annealing. The narrow QPC constriction was defined using electron beam lithography (EBL) and shallow wet-etching on the mesa. The following procedure was used. The sample was flushed in acetone, methanol, and isopropanol before it was ashed in an oxygen plasma for 20 s. The sample was then preetched in 18% HCl for 5 min, flushed in H_2O, and blown dry in nitrogen. It was then prebaked for 5 min at 185 °C before spinning on a 125 nm thick layer of polymethylmethacrylate (pmma) electron beam resist. The EBL pattern was exposed

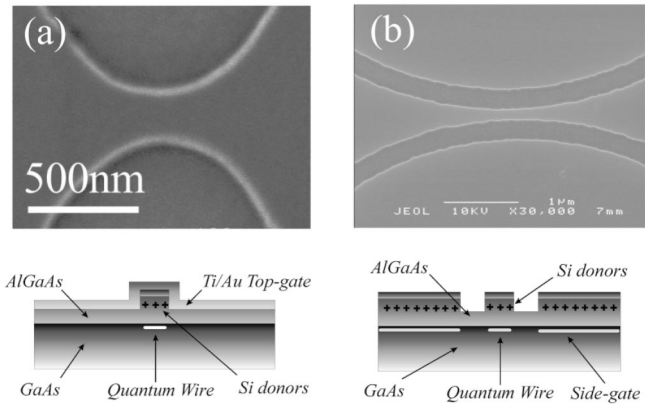

FIG. 1. Scanning electron microscope pictures of the shallow-etched quantum point contacts. (a) Type I devices. The quantum point contact is formed by shallow wet-etching, ~60 nm deep. The etched walls are shaped as two back-to-back parabolas. The picture was recorded before covering the etched constriction with a 10 μm wide, 100 nm thick Ti/Au top gate. (b) Type II and III devices. Two semicircular shaped, etched trenches define the quantum point contact and two large areas of 2DEG, which are used as side gates. In type II devices, the trenches are etched 60 nm deep to remove the donor layer. In type III devices the trenches are etched 90 nm to the GaAlAs/GaAs heterointerface, and subsequently covered with GaAlAs by MBE regrowth.

with an acceleration voltage of 30 kV, and developed in methylisobuthylketone:isopropanol (1:3). The sample was postbaked for 5 min at 115 °C, and ashed for 6 s before etching to 55–60 nm in $H_2O:H_2O_2:H_3PO_4$ (38:1:1) at an etch rate of 100 nm/min.

Three types of devices were investigated: top gated (type I), side gated (type II), and overgrown side gated (type III). Figure 1(a) shows a scanning electron microscope picture of a type I QPC constriction. The shallow etched walls of the constriction are shaped as two back-to-back parabolas. The picture was taken before the constriction was covered by a 10 μm wide, 100 nm thick Ti/Au top-gate electrode. In type II devices, Fig. 1(b), the QPC constriction is formed by etching two semicircular trenches, ~250 nm wide and ~60 nm deep. The etched trenches also define two large areas of 2DEG which are used as side gates. The same pattern is used in type III devices, but the trenches are etched 90 nm deep to reach the GaAs/GaAlAs interface and then MBE regrown. In this way the constriction is bounded by heterostructure interfaces, both vertically and laterally. The electron beam patterning and the MBE regrowth were made before the Ohmic contacts were deposited. Before the regrowth, the sample was desorbed at 630 °C for 2 min in the MBE chamber. The sample was then overgrown with 100 nm undoped $Ga_{0.9}Al_{0.1}As$ and a 5 nm undoped GaAs cap layer, using a growth temperature of 590 °C. The sample parameters are tabulated in Table I.

The samples were mounted in a liquid helium refrigerator, and the differential conductance $G=dI_{sd}/dV_{sd}$ was measured with a small ac excitation voltage, 5–50 μV rms, using standard lock-in techniques at 33–117 Hz. The effective width of the QPC and the electron density inside it is controlled by a gate voltage, which is applied between the source contact and the top or side gate electrode. Henceforth this gate voltage is denoted V_{gs}.

TABLE I. The six quantum point contact samples investigated in this paper. Three types of devices were processed from the same modulation doped GaAs/GaAlAs heterostructure: (I) shallow etch and top gates, (II) shallow-etched trenches, and (III) shallow-etched trenches and MBE regrowth. Geometry related parameters are shown together with the first subband spacing $\varepsilon_1-\varepsilon_0$.

	Sample					
	A	B	C	D	E	F
Type	I	II	II	II	III	III
Width (nm)	200	150	140	110	100	100
Radius (μm)	0.1	2	5	10	2	2
$\varepsilon_1-\varepsilon_0$ (meV)	6.5	7.5	9.7	10.0	5.7	5.9

III. THE LATERAL CONFINEMENT

The shallow-etching technique gives rise to a strong lateral confinement in the constriction, resulting in large separations $\varepsilon_{n+1}-\varepsilon_n$ between the 1D subband edges ε_n. We have previously reported observation of quantized conductance at temperatures above 30 K in a 50 nm wide shallow-etched QPC with a 1D subband energy separation $\varepsilon_1-\varepsilon_0 \approx 20$ meV.[12] In this paper our main example is sample A (type I), but all the measurements reported for this sample have also been performed for the others. Figure 2 shows the gate characteristics, i.e., the differential conductance G, as function of gate-source voltage V_{gs} of sample A, measured at different temperatures. The 200 nm wide, etched QPC constriction is depleted at zero gate voltage, and a positive gate-source voltage is necessary to open it. We estimate the 1D subband energy separations in the QPC's from the thermal smearing of the conductance plateaus, and more precisely by finite bias spectroscopy as described below. For the 200 nm wide QPC constriction in device A we find an energy separation between the two lowest 1D subbands $\varepsilon_1-\varepsilon_0 = 6.5$ meV; see also Table I and Sec. IV B.

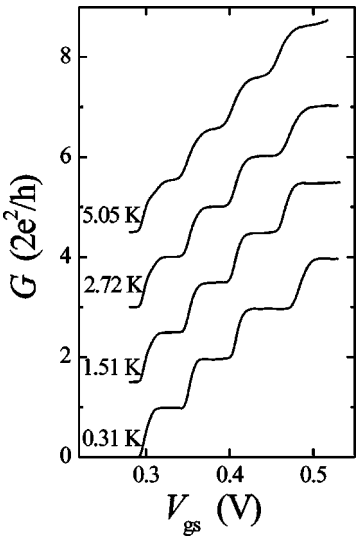

FIG. 2. Conductance versus gate voltage at different temperatures measured on device A. The strong lateral confinement gives a 1D subband energy separation $\varepsilon_1-\varepsilon_0=6.5$ meV. Well-behaved quantized conductance plateaus are observed in the temperature range from 300 mK to above 4 K.

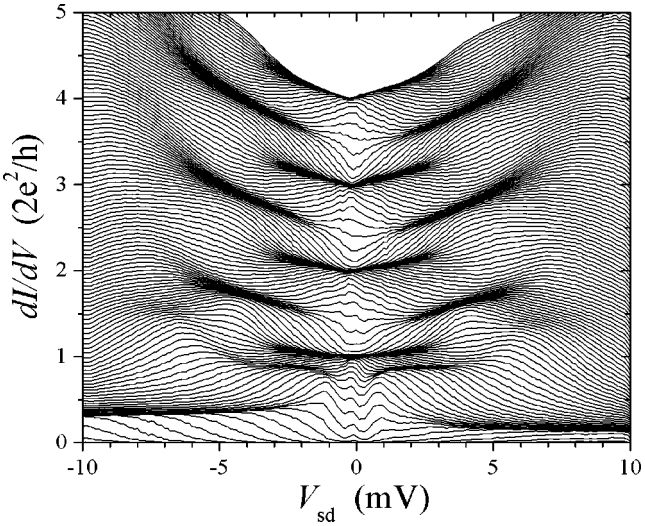

FIG. 3. A plot of the raw data recorded at $T=0.3$ K of the differential conductance dI/dV versus the source-drain bias voltage V_{sd} for sample A. Each trace shows dI/dV as V_{sd} is swept from -10 to 10 mV at fixed gate voltage. The gate voltage is varied in steps of 1 mV. The first four integer conductance plateaus are clearly seen around the vertical line $V_{sd}=0$. Also the corresponding half plateaus are seen for ~ 2 mV$<|V_{sd}|<\sim 6$ mV. A well-developed 0.9 plateau is seen for ~ 1 mV$<|V_{sd}|<\sim 4$ mV, evolving from a rather weak 0.7 anomaly at $V_{sd}\approx 0$ mV. Finally, an additional plateau feature is observed at $G\approx 1.4G_2$ for ~ 6 mV $<|V_{sd}|<\sim 8$ mV.

The confinement potential U determines the transmission properties of the device. It is mainly defined by the sample parameters, the geometry, and the gate-source voltage V_{gs}. However, to some extent, especially near pinch-off where the electron density is low, it does also depend on the bias voltage V_{sd}.[20] In short, we write $U=U(V_{gs},V_{sd})$. This effect of V_{sd} influencing U we denote ''self-gating'' since it resembles the ordinary gate effect from V_{gs}.[21] A sample exhibiting a self-gating can be said to be ''soft;'' if not it is ''rigid.''

The current I through the QPC can be expressed in terms of the transmission functions $\mathcal{T}_n(\varepsilon)$ and the difference $\Delta f(\varepsilon)$ in thermal occupation factors for the source and drain reservoirs as

$$I=\frac{2e}{h}\sum_n \int_{-\infty}^{\infty} d\varepsilon \mathcal{T}_n(\varepsilon)\Delta f(\varepsilon), \tag{1}$$

where

$$\mathcal{T}_n(\varepsilon)=\mathcal{T}_n[\varepsilon,U(V_{gs},V_{sd})], \tag{2}$$

$$\Delta f(\varepsilon)=f[\varepsilon-\mu-\nu eV_{sd}]-f[\varepsilon-\mu+(1-\nu)eV_{sd}], \tag{3}$$

with ν being a number between 0 and 1 describing the ratio of the potential drop on each side of the constriction. Our experimental results are compatible with $\nu=1/2$. Writing explicitly the most relevant functional dependencies for the current, we obtain

$$I=I[U(V_{gs},V_{sd}),\Delta f(V_{sd})]. \tag{4}$$

From this follows to first order in a Taylor expansion the expressions for the differential conductance dI/dV_{sd} and the transconductance dI/dV_{gs}, the quantities measured in the experiments:

$$\frac{dI}{dV_{sd}}\approx\frac{\partial I}{\partial U}\frac{\partial U}{\partial V_{sd}}+\frac{\partial I}{\partial \Delta f}\frac{\partial \Delta f}{\partial V_{sd}}, \tag{5}$$

$$\frac{dI}{dV_{gs}}\approx\frac{\partial I}{\partial U}\frac{\partial U}{\partial V_{gs}}. \tag{6}$$

We note that any sharp feature in the transconductance reminiscent of the characteristic steplike form in the conductance (see Fig. 2) derives from the factor $\partial I/\partial U$ in Eq. (6) relating to the opening of new conductance channels. The other factor $\partial U/\partial V_{gs}$ is just varying smoothly due to its origin in electrostatics over length scales of the order of at least 100 nm. But $\partial I/\partial U$ also appears as a prefactor in the first term of the differential conductance in Eq. (5). Thus the self-gating effect is enhanced when the transconductance is large. Conversely, at low temperatures at the middle of a plateau the current is almost unaffected by changes in U; at least only very smooth changes are expected. If $\partial I/\partial U$ can be neglected, the differential conductance is given by the occupation factor related second term in Eq. (5). As the temperature is enhanced the transconductance becomes more important even at the center of the plateau as is evident for the highest temperatures in Fig. 7.

IV. BIAS SPECTROSCOPY AND THE ENERGY DIFFERENCE Δ

An important source of information about the energy subbands in a QPC is finite bias spectroscopy. We use the technique developed by Patel *et al.*[8] and described theoretically by Glazman and Khaetskii.[22] The differential conductance $G=dI/dV_{sd}$ at finite dc source-drain bias voltage V_{sd} is measured by lock-in technique, using a small ac signal, 50 μV rms and 117 Hz, superposed on the dc source-drain bias voltage.

A. The differential conductance at finite bias

In Fig. 3 the dependence at $T=0.3$ K of the differential conductance of sample A on the dc source-drain bias is shown. For each trace the gate voltage is fixed, while going from one trace to the next represents an increase in gate voltage of 1 mV. Conductance plateaus appear as dark regions with a high density of traces. Four types of plateau are observed in the data. (1) The first four integer conductance plateaus are clearly seen at $G=nG_2$ around $V_{sd}=0$. (2) The corresponding half plateaus[23,24] at approximately $(n-1/2)G_2$ appear for bias voltages ~ 2 mV$<|V_{sd}|<\sim 6$ mV, when the chemical potential of one reservoir lies above the edge of one subband, while the other potential lies below. (3) We remark that the 0.7 structure is observed near $V_{sd}=0$. As the source-drain bias is increased, the G value of the conductance anomaly increases, and for $|V_{sd}|\approx 1$ mV the anomaly has evolved into a well-defined plateau with a conductance G between $0.8G_2$ and $0.9G_2$. (4) Finally, an additional plateau feature is observed at $G\approx 1.4G_2$ for ~ 6 mV $<|V_{sd}|<\sim 8$ mV.

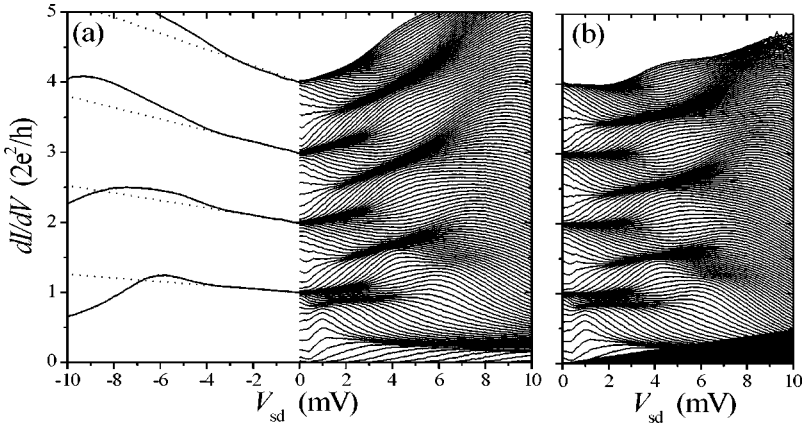

FIG. 4. (a) The symmetrized plot of the differential conductance. In the right half are shown all the conductance traces, while in the left part are shown only the four center plateau traces (full lines) together with the best fit (dotted lines) to the form Eq. (8). (b) The symmetrized plot after subtraction of the V_{sd} dependence due to self-gating.

From the data in Fig. 3 it is seen that the differential conductance depends rather strongly on V_{sd}. For the lowest conductances a pronounced asymmetry is observed: for negative V_{sd} the conductance is higher than for positive V_{sd}. This effect is always seen when the gate bias is applied relative to the source contact. It persists in all samples even for different grounding points. Furthermore, even at the smallest source-drain bias we observe a strong nonlinearity in the conductance at the middle of the integer plateaus, where the chemical potentials lie in the middle of the gap between 1D subband edges: the integer plateaus in Fig. 3 are not flat around $V_{sd}=0$. In the following we interpret this nonlinearity and the asymmetry in terms of the self-gating effect presented in Sec. III. We subtract this trivial effect from the data to obtain data corresponding to a ''rigid'' QPC not subject to self-gating.

First we treat the asymmetry of the data, which is strongest for the lowest values of V_{gs} or equivalently for the lowest electron densities. A simple reason for this can be found in the electrostatics of the QPC. We notice that $\partial I/\partial U$ is always antisymmetric with respect to V_{sd}. However, since the gate voltage is applied relative to the source contact, no special symmetry relations are expected in $\partial U/\partial V_{sd}$ as the polarity V_{sd} is changed. Especially near pinch-off when the electron density is low in the QPC, the effect of a polarity change in V_{sd} can be important. Thus we expect on general grounds that, regarded as a function of V_{sd}, the term $(\partial I/\partial U)(\partial U/\partial V_{sd})$ from Eq. (5) contains both a symmetric and an antisymmetric part. This conclusion holds true for any value of the ratio ν of the voltage drop in Eq. (3), in contrast to Ref. 20, where $\nu \neq 1/2$ had to be adopted to explain the asymmetry. The antisymmetric part thus attributed to rather trivial electrostatics is subtracted from the data by forming the symmetric combination

$$I(|V_{sd}|) \equiv \tfrac{1}{2}[I(+V_{sd}) + I(-V_{sd})]. \tag{7}$$

Next we focus on the four dI/dV_{sd} traces which for $V_{sd}=0$ go right through the center of each of the first four integer conductance plateaus. As mentioned in Sec. III no appreciable self-gating effect is expected here. Only smooth changes with V_{gs} are expected for moderate values of the bias V_{sd}. Using a second order Taylor expansion of dI/dV_{sd} in V_{sd} we extend Eq. (5) to the form

$$\frac{dI}{dV_{sd}} \approx (\alpha V_{gs} + \beta) + (\alpha' V_{gs} + \beta') V_{sd}, \tag{8}$$

and fit the four parameters α, β, α', and β' to the four mid-plateau traces. We then subtract from all the traces the fitted V_{sd} dependence. The result of this procedure is shown in Fig. 4. We end up with plots of the integer plateaus in the differential conductance that for moderate values of V_{sd} up to 2–3 mV are independent of the finite bias voltage. Note how the 0.9 anomalous plateau has also now become flat. We can thus unambiguously assign constant values for the conductance plateaus in a wide range. The half plateaus, however, still show a dependence on the bias voltage, although not as strongly as before, indicating the large influence of V_{sd} on the potential U in the strongly nonequilibrium case where one reservoir is injecting electrons above the topmost subband edges and the other is not. We note that experimentally we never see $G=0.5$ at the first half plateau but rather a value substantially below; and it is never quite constant but decreasing with increasing bias; in the present case $G \approx 0.3$. This is probably due to the intricate self-consistent electrostatic effects at pinch-off, but this has to be investigated further. The measured values of the conductance at the plateaus are discussed further in Sec. IV C.

B. The transconductance

To display the features in the conductance traces more clearly we study the transconductance dG/dV_{gs}, which is calculated by numerical differentiation from the measured differential conductance $G=dI/dV_{sd}$. The transconductance is zero (or small) on conductance plateaus and shows peaks in the transition regions between plateaus. In Fig. 5 is shown a gray scale plot of the transconductance of sample A, calculated from the data in Fig. 3. The plot covers the range -10 to 10 mV in source-drain bias and 0.25 to 0.50 V in gate voltage, corresponding to the first four integer conductance plateaus. Plateau regions (small transconductance) appear as light regions bounded by dark transition regions (high transconductance). The main features of the plot are the well-known diamond shaped dark transition regions surrounding the integer plateaus nG_2 and the half plateaus $(n-1/2)G_2$, where $n=1,2,\ldots$.[9,14] The transitions in G are due to the crossing of the chemical potentials μ_s and μ_d of the source and drain reservoirs through the subband edges defining the transmitting subbands. The procedure described

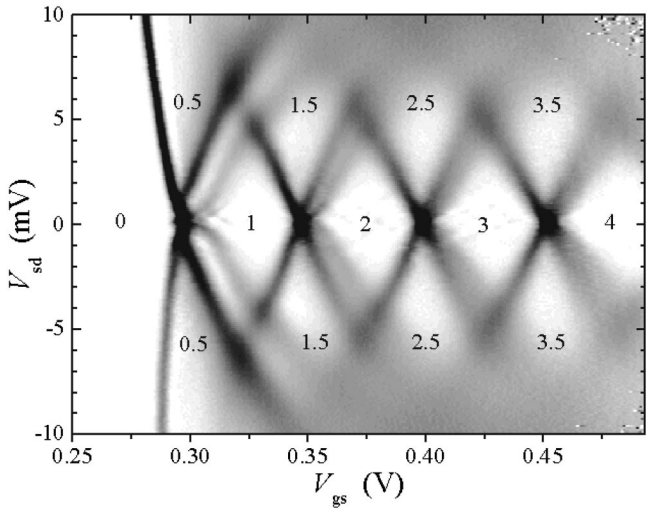

FIG. 5. Gray scale plot of the transconductance dG/dV_{gs} versus gate voltage V_{gs} and bias voltage V_{sd} for sample A at $T=0.3$ K. White corresponds to zero transconductance, i.e., to plateaus in the differential conductance $G=dI/dV_{sd}$. Black corresponds to high transconductance. The dark lines in the plot therefore indicate the positions (V_{gs},V_{sd}) of transitions between the various conductance plateaus. The numbers indicate the value of G in units of $2e^2/h$ on the various plateaus.

in Sec. IV A to get rid of the V_{sd} dependence of the plateau values allows for an unambiguous assignment of conductance values in each of the diamonds of the transconductance plot. The subband separations $\varepsilon_{n+1}-\varepsilon_n$ are extracted from the main diamond structure by reading off the value of V_{sd} where the straight black lines surrounding the $G=n$ diamond intersect, indicating the appearance of the next subband. The first intersection is at $(V_{gs},V_{sd})=(0.32\text{ V},6.5\text{ mV})$. Thus $\varepsilon_1-\varepsilon_0=6.5$ mV as listed in Table I.

C. The anomalous subband edge ε_0' and $\Delta(V_{gs})$

In addition to the main feature, anomalous conductance plateaus are seen. The most pronounced is the anomalous $G=0.9$ plateau, which appears in the left-hand side of the $G=1$ diamond between the leftmost black straight edge and a curved gray anomalous transition line. Note how the anomalous transition line is continued smoothly into the $G=1.5$ diamond. Similar, but much weaker, anomalous structures are seen running inside the $G=2$ diamond continuing into the $G=2.5$ diamond, and inside the $G=3$ diamond continuing into the $G=3.5$ diamond.

Just as the black straight lines in the gray scale plot of Fig. 5 are due to the crossing of μ_s and μ_d through the ordinary subband edges ε_n, it is tempting to associate the anomalous transitions with the crossing of anomalous subband edges ε_n'. In particular, the strong transition ridge between the 1.0 and 0.9 plateaus can be analyzed in those terms. In the standard theory, changing V_{sd} for fixed V_{gs} in the first half of the first plateau leads to the sequence $G=1.0\rightarrow G=0.5$, since μ_d drops below the lowest lying spin-degenerate subband edge. However, this sequence is not observed in the measurements. To make this point clear we show in Fig. 6 four individual traces at fixed V_{gs}, denoted A to D, and four traces at fixed V_{sd}, denoted E to H. In Fig. 6(a) these traces are drawn as dashed lines in the V_{gs}-V_{sd} plane. In Fig. 6(b) is shown the differential conductance along traces A to D. The zero bias point of these four traces corresponds to the following positions on the $T=0.3$ K conductance curve of Fig. 2: below the first plateau (A), on the lower half of the first plateau (B), on the upper half of the first plateau (C), and on the lower half of the second plateau (D). First follow trace B. It exhibits the plateau sequence $G=1.0\rightarrow G=0.85\rightarrow G=0.2$. Probably due to the ''softness'' of the QPC at low electron densities, the value of the ''0.5 plateau'' is around 0.2, where the trace meet with trace A evolving from $G=0$ into a plateau at $G=0.15$. It is as if the conductance in trace B drops in two steps corresponding to the crossing of two subband edges rather than just one, perhaps as a consequence of lifting of the spin degeneracy in the QPC.[7,16,18]

It seems quite natural to associate the anomalous transition with an anomalous subband edge ε_0' split off from and

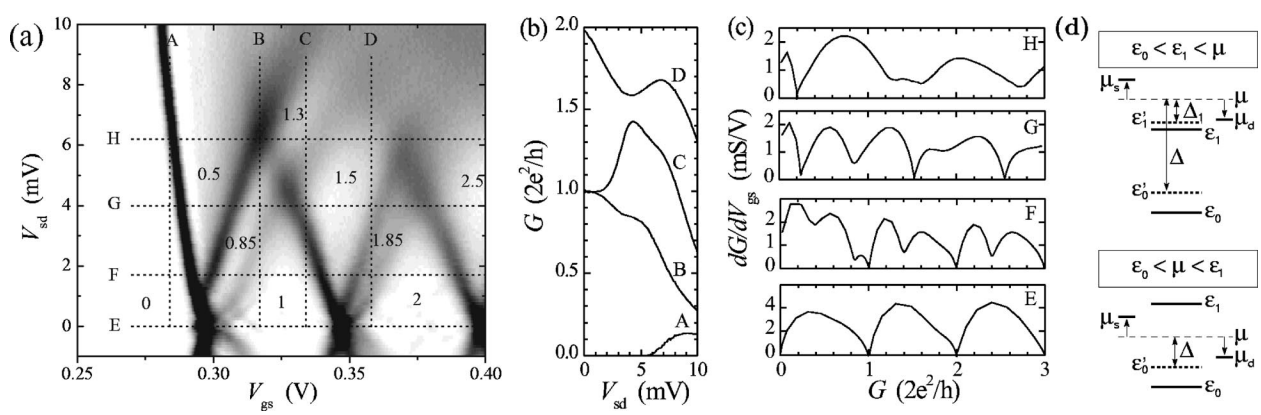

FIG. 6. (a) A section of the gray scale plot from Fig. 5 displaying the four vertical V_{sd} scan lines A, B, C, and D of panel (b) below and the four horizontal V_{gs} scan lines E, F, G, and H of panel (c) below. (b) The differential conductance G versus bias voltage V_{sd} for four different fixed values of the gate voltage corresponding to positions A before the first conductance plateau, B on the lower half of the same plateau, C on the upper half of it, and D on the lower half of the second plateau. (c) The transconductance dG/dV_{gs} versus the differential conductance $G=dI/dV_{sd}$ at four different bias voltages $V_{sd}=0$, 1.7, 4.0, and 6.2 mV, traces E, F, G, and H, respectively. (d) illustrates a model involving ordinary subband edges ε_n and anomalous ones ε_n'. The ε_n' splits off from ε_n only for $\mu=(\mu_s+\mu_d)/2>\varepsilon_n$. Changing $\mu_s-\mu_d=eV_{sd}$ in the lower (upper) panel corresponds to scanning along trace C (D). Note how ε_0' gives rise to the anomalous ridge through the 1 and 1.5 diamonds, and ε_1' to that in the 2 diamond.

lying above the ordinary subband edge ε_0, which therefore is encountered first by μ_d as the bias voltage $(\mu_s-\mu_d)/e$ is raised [see Fig. 6(d)]. This would also account for the continuation of the anomalous transition into the 1.5 diamond as seen by studying the behavior of trace C. Increasing V_{sd} from 0, this trace exhibits a clear plateau at 1.0 before it rises and develops into a plateau at $G=1.45$ as μ_s is raised above the second subband ε_1. For slightly larger values of V_{sd}, μ_d falls below the anomalous subband edge ε_0'; G drops and the trace exhibits a shoulderlike feature around $G=1.3$. Only for yet higher values of V_{sd} does μ_d drop below the ordinary first subband ε_0 leading to $G=1$ and lower values as in the standard case. Thus as a function of the bias voltage V_{sd} the plateau sequences $G=1.0\rightarrow G=0.5$ and $G=1.0\rightarrow G=1.5\rightarrow G=1.0$, for the first and second halves of the $G=1$ plateau, expected from the simple half plateau model, in experiment are seen rather to be $G=1.0\rightarrow G=0.85\rightarrow G=0.5$ and $G=1.0\rightarrow G=1.5\rightarrow G=1.3\rightarrow G=1.0$.

The values of the conductance at the plateaus are found after the fitting procedure described in Fig. 4. The most precise way to obtain these values is through Fig. 6(c), where the transconductance dG/dV_{gs} is plotted versus the differential conductance G at four different but fixed bias voltages, traces E, F, G, and H. The plateaus appear as minima in the curves, since a minimum in the the transconductance correspond to the point of least slope in plots of G versus V_{gs}. Ideally, if the plateaus are completely flat, the values at the minima are 0. This happens, for example, at the integer plateaus seen in trace E and the half plateaus in trace G. The 0.85 plateau is never completely flat, but in traces F and G it is seen as a well developed minimum.

For comparison with the temperature data presented in Sec. VI we introduce the anomalous gate-voltage-dependent (and hence density-dependent) energy difference $\Delta(V_{gs})$. It is related to that particular gate-voltage-dependent value V_{sd}^* of the source-drain bias that maximizes the transconductance along the 0.9-1.0 and 1.35-1.5 ridges in the gray scale plot:

$$\Delta(V_{gs})=\frac{1}{2}eV_{sd}^*(V_{gs}). \tag{9}$$

In terms of an anomalous subband, Δ is interpreted as the difference $\mu-\varepsilon_0'$ between the chemical potential μ and the anomalous subband edge ε_0' as outlined in Fig. 6(d). In Fig. 5 it is seen that similar ridges appear, progressively weaker, for the higher subbands. The weakening of the effect may be due to less pronounced spin polarization at the higher densities present when more subbands are occupied.[16] Finally, we note that, in contrast to the normal n plateaus, the anomalous n' plateaus can appear only when $\mu=(\mu_s-\mu_d)/2$ is above a given ordinary subband edge ε_n, i.e., the anomalous plateaus appear only in the left-hand sides of the diamonds in the gray scale plots. This is another indication that the anomalous plateaus are related to interaction effects and not to simple single-particle subband effects.

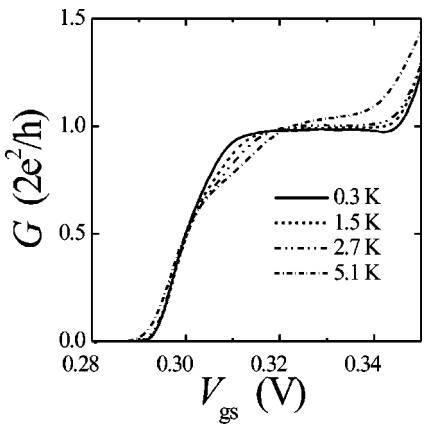

FIG. 7. The conductance versus gate voltage of sample A at the first quantized conductance plateau, measured at different temperatures from 0.3 K to 5.1 K. As the temperature is raised, the 0.7 anomaly emerges as a suppression of conductance in the first half of the conductance plateau, while the other half remains flat.

V. THE ACTIVATION TEMPERATURE T_A

To gain further insight into the conductance anomaly we also study the temperature development of the first conductance plateau $G=G_2$. In Fig. 7 is shown a set of measurements performed on sample A. At the lowest temperature, 0.3 K, the plateau is broad and flat. With a 1D subband energy separation of 6.5 meV, the thermal smearing of the plateau should be negligible at temperatures below 4 K. This is indeed also the case for the upper half of the conductance plateau, $V_{gs}\simeq 320$–340 mV, which stays flat as the temperature is raised. On the lower half of the plateau, the conductance is suppressed below the plateau value G_2 as the temperature is raised, developing a plateaulike structure around the conductance value $0.7G_2$. This is the 0.7 conductance anomaly.

The large 1D subband energy separation in shallow-etched QPC's allows us to study the temperature dependence of the 0.7 structure at temperatures up to around 5 K without appreciable thermal smearing of the quantized conductance. In Fig. 8 we present two Arrhenius plots of the conductance suppression shown in Fig. 7 at $V_{gs}=0.305$ V and 0.309 V.

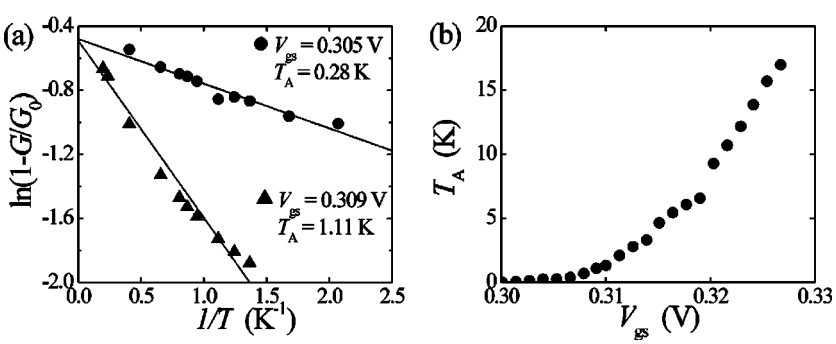

FIG. 8. (a) Temperature dependence of the conductance suppression $G_0-G(T)$ at fixed gate voltages $V_{gs}=0.305$ V and 0.309 V, measured on device A. The data show Arrhenius behavior, $G(T)/G_0=1-C\exp(-T_A/T)$, with an activation temperature T_A. (b) The measured activation temperature T_A as function of gate voltage across the $0.7G_2$ structure, measured on device A.

We plot the relative conductance suppression $1-G(T)/G_0$ (where G_0 is the measured conductance value of the plateau) versus $1/T$ at the given fixed gate voltage. The linear behavior in the semilogarithmic Arrhenius plot indicates an activated behavior, $G(T)/G_0=1-C\exp(-T_A/T)$, with the corresponding activation temperatures $T_A=0.28$ K and 1.11 K extracted from the two slopes. Figure 8(b) shows how the measured activation temperature T_A as a function of gate voltage increases from 0 at pinch-off to a few kelvin in the middle of the conductance plateau.

In the usual framework of the Landauer-Büttiker formalism the observed activated suppression of the conductance indicates that the 0.7 structure is associated with thermal depopulation of a subband having a gate-voltage-dependent subband edge ε_n'. If a subband edge lies $k_BT_A(V_{gs})$ below the Fermi level, an activated behavior is indeed seen in G. A phenomenological theory along these lines has been presented by Bruus *et al.*[18] Moreover, this picture is in accordance with the discussion presented in Sec. IV C of the crossing of subband edges ε_n and ε_n' at finite bias. In the following analysis we connect the measured activation temperature with the energy gap Δ found by finite bias spectroscopy.

VI. COMPARING Δ AND T_A

It is possible to ascribe the same origin to the appearance of the plateau at $0.9G_2$ at finite bias as to the 0.7 anomaly. The two effects are connected by the energies $\Delta(V_{gs})$ and $T_A(V_{gs})$. Consider a fixed gate voltage on the lower half of the G_2 plateau. The data are taken at low temperature. At zero bias the excitation energies available for the electrons at the Fermi energy are not sufficient to reach the subband edge lying k_BT_A below the Fermi level, and the conductance has the expected, quantized value G_2. As the source-drain bias voltage $V_{sd}=(\mu_s-\mu_d)/e$ is increased, we assume that half the potential drop is before and the other half after the QPC, i.e., $\nu=1/2$ in Eq. (3). The electrons from the drain reservoir are injected below the subband edge when $eV_{sd}/2=k_BT_A$. This assumption is supported by our experiments. In Fig. 9 we have plotted for all six samples the expected position of the resonance $V_{sd}^*=2k_BT_A/e$ versus gate voltage as white circles. The activation temperature used in this plot is obtained from the measured temperature dependence of the 0.7 structure, like the one presented in Figs. 7 and 8. As seen from Fig. 9 the transition from the regular G_2 plateau to the anomalous $0.85G_2$ plateau appears at the expected resonance position.

The quality of the 0.7/0.85 anomalies is varying a lot from sample to sample. The exact reason for this is not known at present. One can think of many reasons such as impurities, geometry related defects, and other sample parameters. But it is noteworthy that for *all* samples the energy $\Delta(V_{gs})$ characterizing the 0.85 anomaly coincides with the activation energy k_BT_A deduced from the 0.7 anomaly.

VII. CONCLUSION

We have investigated the 0.7 conductance anomaly in six samples of three different types of shallow-etched GaAs/GaAlAS QPC: top gated, side gated and overgrown side gated. We note that the QPC confinement potential U depends on both V_{gs} and V_{sd}. The influence of V_{sd}, referred to as self-gating, can explain the distinct asymmetry and nonlinearity always observed in the differential conductance of QPC's. The QPC's thus appear to be ''soft,'' but we have shown how to subtract the self-gating effect from the data. Based on finite bias spectroscopy we have presented experimental evidence that the 0.7 anomaly is associated with a density-dependent energy difference $\Delta=\mu-\varepsilon_0'$ of the order of a few kelvin, the distance from the chemical potential μ to an anomalous subband edge ε_0'. The shallow-etching technique gives rise to a strong lateral confinement with 1D subband energy separations of 5–20 meV. We have therefore been able study the 0.7 anomaly for higher temperatures than for normal split-gate devices, and this allowed a detailed study of the temperature dependence of the conductance anomaly. We have found an activated behavior of the conductance suppression at the 0.7 anomaly, with a density-dependent activation temperature T_A of a few kelvin. For all six samples the energy difference Δ is found to be equal to the activation energy k_BT_A. Our observations support the idea that the 0.7/0.85 conductance anomaly arises from the existence of an anomalous subband edge in the QPC. The nature of the anomalous subbands is presently unknown, but bour observation that the anomalous plateaus appear only when both μ_s and μ_d are above a given subband edge, and the behavior of the 0.7 anomaly as a function of magnetic field,[7] indicate the importance of interaction effects beyond

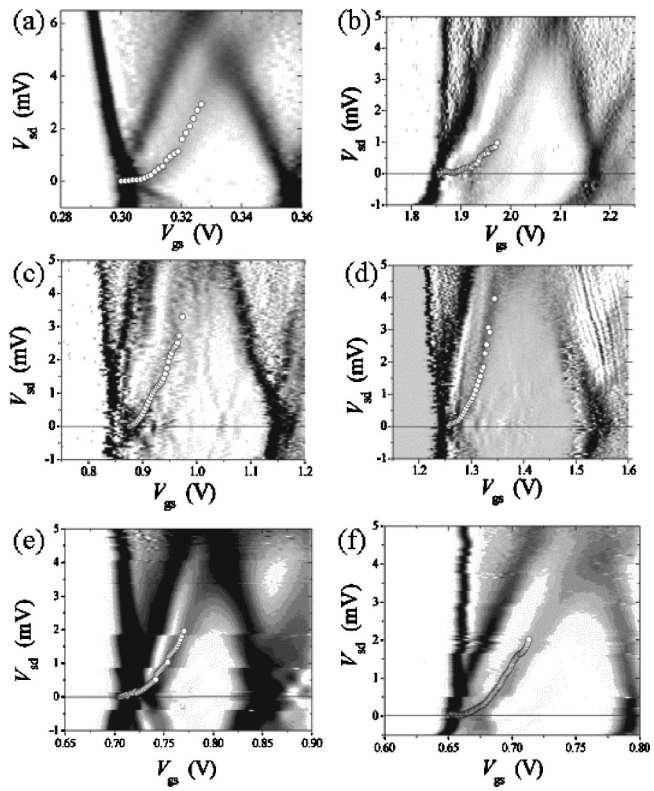

FIG. 9. Gray scale plots as in Fig. 5 of the differential transconductance for all six samples A–F of Table I. The open circles are the data points $(V_{gs}, 2k_BT_A/e)$ where the activation temperature T_A was extracted from the measured temperature dependence of the zero-bias conductance.

the simple single-particle subband picture, presumably related to spin polarization.[7,16,18]

ACKNOWLEDGMENTS

This research is part of the EU IT-LTR program Q-SWITCH (Grant Nos. 20960/30960), and was partly supported by the Danish Technical Research Council (Grant No. 9701490) and by the Danish Natural Science Research Council (Grant Nos. 9502937, 9600548, and 9601677). The III-V materials used in this investigation were made at the III-V Nanolab, operated jointly by the Microelectronics Center of the Danish Technical University and the Niels Bohr Institute fAPG, University of Copenhagen.

[1] B.J. van Wees, H. van Houten, C.W.J. Beenakker, J.G. Williamson, L.P. Kouwenhoven, D. van der Marel, and C.T. Foxon, Phys. Rev. Lett. **60**, 848 (1988).

[2] D.A. Wharam, T.J. Thornton, R. Newbury, M. Pepper, H. Ahmed, J.E.F. Frost, D.G. Hasko, D.C. Peacock, D.A. Ritchie, and G.A. Jones, J. Phys. C **21**, L209 (1988).

[3] H. Van Houten, C.W.J. Beenakker, and B. van Wees, in *Nanostructured Systems*, edited by M. Reed, Vol. 35 of *Semiconductors and Semimetals*, edited by R.K. Williamson, A.C. Beer, and R. Weber (Academic Press, San Diego, 1992), p. 9.

[4] S. Tarucha, T. Honda, and T. Saku, Solid State Commun. **94**, 413 (1995).

[5] A. Yacobi, H.L. Stormer, N.S. Wingreen, L.N. Pfeiffer, K.W. Baldwin, and K.W. West, Phys. Rev. Lett. **77**, 4612 (1996).

[6] R.D. Tscheuschner and A.D. Wieck, Superlattices Microstruct. **20**, 615 (1996).

[7] K.J. Thomas, J.T. Nicholls, M.Y. Simmons, M. Pepper, D.R. Mace, and D.A. Ritchie, Phys. Rev. Lett. **77**, 135 (1996).

[8] N.K. Patel, J.T. Nicholls, L. Martin-Moreno, M. Pepper, J.E.F. Frost, D.A. Ritchie, and G.A.C. Jones, Phys. Rev. B **44**, 13 549 (1991).

[9] K.J. Thomas, J.T. Nicholls, N.J. Appleyard, M. Pepper, M.Y. Simmons, D.R. Mace, W.R. Tribe, and D.A. Ritchie, Phys. Rev. B **58**, 4846 (1998).

[10] C.-T. Liang, M.Y. Simmons, C.G. Smith, G.H. Kim, D.A. Ritchie, and M. Pepper, Phys. Rev. B **60**, 10 687 (1999).

[11] K.J. Thomas, J.T. Nicholls, M. Pepper, W.R. Tribe, M.Y. Simmons, and D.A. Ritchie, Phys. Rev. B **61**, R13 365 (2000).

[12] A. Kristensen, J.B. Jensen, M. Zaffalon, C.B. Sørensen, S.M. Reimann, P.E. Lindelof, M. Michel, and A. Forchel, J. Appl. Phys. **83**, 607 (1998).

[13] A. Kristensen, P.E. Lindelof, J.B. Jensen, M. Zaffalon, J. Hollinghery, S.W. Pedersen, J. Nygård, H. Bruus, S.M. Reimann, C.B. Sørensen, M. Michel, and A. Forchel, Physica B **249-251**, 180 (1998).

[14] A. Kristensen, H. Bruus, A. Forchel, J.B. Jensen, P.E. Lindelof, M. Michel, J. Nygård, and C.B. Sørensen, cond-mat/9808007 (unpublished).

[15] D.J. Reilly, G.R. Facer, A.S. Dzurak, B.E. Kane, R.G. Clark, P.J. Stiles, J.L. O'Brien, N.E. Lumpkin, L.N. Pfeiffer, and K.W. West, cond-mat/0001174 (unpublished).

[16] C.-K. Wang and K.-F. Berggren, Phys. Rev. B **57**, 4552 (1998).

[17] B. Spivak and F. Zhou, Phys. Rev. B **61**, 16 730 (2000).

[18] H. Bruus, V.V. Cheianov, and K. Flensberg, cond-mat/0002338 (unpublished).

[19] B.E. Kane, G.R. Facer, A.S. Dzurak, N.E. Lumpkin, R.G. Clark, L.N. Pfeiffer, and K.W. West, Appl. Phys. Lett. **72**, 3506 (1998).

[20] L. Martin-Moreno, J.T. Nicholls, N.K. Patel, and M. Pepper, J. Phys.: Condens. Matter **4**, 1323 (1992).

[21] The self-gating resembles the so-called channel length modulation well known from conventional field effect transistors.

[22] L.I. Glazman and A.V. Khaetskii, Europhys. Lett. **9**, 263 (1989).

[23] N.K. Patel, L. Martin-Moreno, M. Pepper, R. Newbury, J.E.F. Frost, D.A. Ritchie, G.A.C. Jones, J.T.M.B. Janssen, J. Singleton, and J.A.A.J. Perenboom, J. Phys.: Condens. Matter **2**, 7247 (1990).

[24] L.P. Kouwenhoven, B.J. van Wees, C.J.P.M. Harmans, J.G. Williamson, H. van Houten, C.W.J. Beenakker, C.T. Foxon, and J.J. Harris, Phys. Rev. B **39**, 8040 (1989).